Received: 7 September 2018 | Revised: 1 December 2018 | Accepted: 18 December 2018

DOI: 10.4218/etrij.2018-0502

SPECIAL ISSUE

WILEY ETRI Journal

Visual perception of Fourier rainbow holographic display

Hyon-Gon Choo[1] | **Maksymilian Chlipala**[2] | **Tomasz Kozacki**[2]

[1]Broadcasting and Media Research Laboratory, Electronics and Telecommunications Research Institute, Deajeon, Rep. of Korea.

[2]Photonics Engineering Division, Warsaw University of Technology, Warsaw, Poland.

Correspondence
Hyon-Gon Choo, Broadcasting and Media Research Laboratory, Electronics and Telecommunications Research Institute, Deajeon, Rep. of Korea.
Email: hyongonchoo@etri.re.kr

Funding information
This work was supported by the Cross-Ministry Giga KOREA Project (GK18D0100, GigaKOREA); statutory founds of Warsaw University of Technology.

The rainbow hologram provides views of reconstruction with rainbow color within a large viewing zone. In our recent paper, a Fourier rainbow holographic display using diffraction grating and a white-light LED source was introduced. In this technique, the rainbow effect is realized by the dispersion of white-light source on diffraction grating, while the slit is implemented numerically by reducing the demands of the space-bandwidth product of the display. This paper presents a novel analysis on the visual perception of the Fourier rainbow holographic display using Wigner distribution. The view-dependent appearance of the image, including multispectral field of view and viewing zone, is investigated considering the observer and the display parameters. The resolution of the holographic view is also investigated. For this, a new quantitative assessment for image blur is introduced using Wigner distribution analysis. The analysis is supported with numerical simulations and experimentally captured optical reconstructions for the holograms of the computer model and real object generated with different slit size, reconstruction distance, and different observation conditions.

KEYWORDS
hologram, holographic display, rainbow hologram, Wigner distribution

1 | INTRODUCTION

Holography is an effective technique for realizing a 3D display. It provides real 3D reconstructions with all physiological depth cues, which drives human interaction as in a real world. The recent development of the display technology has resulted in holography increasingly attracting general audience and scientific community [1].

A holographic display should provide attractive images, which can be comfortably observed. The first condition is met when the display reconstructs large, high-quality images, and the second condition is met when this image can be observed from a large viewing zone. In digital holography, the amount of information that can be reproduced by the display is determined by the space-bandwidth product (SBP) of the used spatial light modulator (SLM). Since the currently available SLMs have small SBP, their direct application does not allow to obtain large size reconstruction and a large viewing zone simultaneously; the extension of one always takes place at the expense of the other. Therefore, methods that increase SBP of a holographic display are of utmost importance.

One solution to increase SBP is developing an SLM with more pixels. However, this requires a fully integrated technological chain solution, including the construction of the SLM, data processing, transmission, and storage. For these reasons, many approaches utilize multiple SLMs. One solution is to use numerous SLMs in circular configuration [2,3]. This allows to enlarge the viewing zone of the display and observe the entire scene with naked eye; however, its size must be smaller than that of the SLM. Multiple SLMs can also be arranged in a 2D matrix to enlarge the object size [4,5]. Different methods employ high-speed SLMs and time multiplexing with a scanning system in one or both directions [6–8] for further extension of the viewing zone. This requires a high-speed SLM, and thus, a digital micromirror device (DMD) is especially suitable. It works with frequencies above 20 kHz. However, since a DMD is a binary type of modulator, the quality of reconstructed objects is decreased. Since among all listed solutions, the number of real/virtual SLMs is high, the systems are complicated, difficult to build, and expensive.

An interesting and practical approach, which allows for the observation of large objects, is a viewing window (VW) method [9]. In this imaging technique, by using a field lens placed in the display output, it is possible to see a large scene with naked eye, however within a narrow angular range. Thus, the observation position is very small and the method must be supported by spatial/temporal multiplexing [6,10–12] or an eye tracking system [13].

Another suitable solution to the limited SBP problem is to decrease the SBP requirement of the display. A way to achieve this is to apply the horizontal parallax only (HPO) concept. Since the vertical parallax of the object is removed in this method, the amount of information that has to be reproduced by the display is reduced. A well-recognized and established HPO approach for this purpose is rainbow holography [14]. In this solution, a physical slit is imposed on the recorded hologram and a sharp and bright 3D reconstruction is observed when using white-light illumination. Most of the studies on digital rainbow holography have concentrated on computer generated holograms (CGHs) [15,16], as the rainbow technique allows to reduce the computation effort. Nevertheless, the key advantage of applying the rainbow holography concept in a holographic display is the enlarged viewing zone. Recently, a Fourier rainbow holographic display (FRHD) utilizing high-frequency diffraction grating and a white LED source have been presented [17]. In this technique, the slit is implemented numerically by reducing the frequency range of the hologram, while the rainbow effect is realized through angular multiplexing by the white-light spectrum dispersed on the diffraction grating.

The rainbow display allows the reconstruction of large 3D orthoscopic objects. Even though it is not reproducing colors, the perceived image looks interesting and impressive. The display provides views where colors and resolution depend on the dimension and position of the observer's eye pupil. Therefore, in rainbow holography, visual perception plays a very important role.

In this study, we analyze the visual perception of the FRHD using Wigner distribution (WD). The preliminary and experimental investigations of visual properties of the FRHD can be found in our previous report [18]. Here, we extend this analysis theoretically, numerically, and experimentally. The first aspect of the study investigates the viewpoint-dependent appearance of an image, including multispectral field of view (FoV) and a viewing zone. The second aspect concerns image blur, which is a measure of resolution for rainbow holography [19]. For this purpose, we employ WD representation [20], which is a useful tool for studying 3D imaging of a holographic display. In [21], WD was employed for investigating the resolution and visual perception of 3D holographic displays with a single SLM. The analysis was extended to the VW display [22] and multiple SLM displays with an enlarged viewing zone [23]. These studies concern holographic reconstructions for a single color. Nevertheless, they can be easily extended to an RGB display. In the FRHD, a single hologram is reconstructed with multiple plane waves of different wavelengths and the eye collects reconstructions of specific range of wavelengths, which depends on the pupil size and position. Therefore, the WD analysis of the FRHD is not straightforward. For this reason, a novel framework using WD analysis is proposed, which is used to investigate the propagation of a holographic signal, including the effect of SLM bandwidth, rainbow illumination, and eye pupil. The investigations provide generalized measures of resolution of the view and multispectral properties of the view within the viewing zone.

In Section 2, we review the FRHD briefly. In Section 3, visual properties of the display are discussed. In Section 4, experimental results are shown. We conclude this study in Section 5.

2 | FOURIER RAINBOW HOLOGRAPHIC DISPLAY

In this section, we briefly review the FRHD [17]. It is a combination of the VW display, an external rainbow illumination, and numerical processing. Figure 1 shows a simplified structure of the FRHD. In the VW display, a large hologram can be observed only when the observer's eye is placed exactly at the position of the VW, which is formed around the focus point of a field lens. The FRHD employs diffraction grating in the illumination module to provide SLM illumination with different angles of incidence for different wavelength components. As a result, for each wavelength, the position of the VW is shifted along the focal plane of a field lens, as depicted in Figure 1. This forms the rainbow VW (RVW) and extends the viewing zone of the display in vertical and longitudinal directions. In the VW display, when the observer's eye is out of the VW, no reconstruction is observed. On the contrary, the FRHD provides views of entire reconstruction, also in a large range of the observer's positions.

Figure 2 illustrates the FRHD setup. In our implementation, a white-light pigtailed LED with 960 μm fiber core is used as the light source. It is placed at the focal plane of the collimating lens L_C (F_C = 300 mm), which forms plane wave illumination. Next, the beam hits the diffraction grating DG at angle θ in vertical direction. The angle θ is set using the mirror to obtain normal direction of illumination

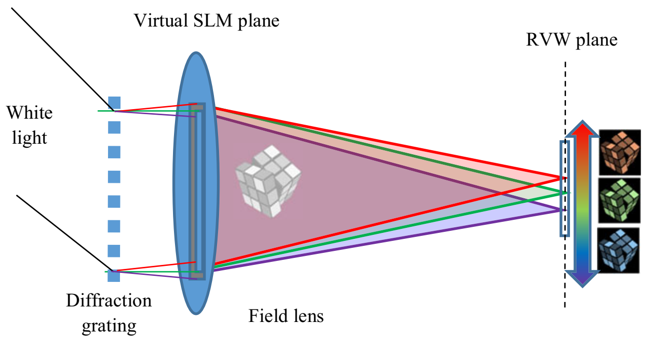

FIGURE 1 Concept of FRHD

for the -1st order of diffraction grating, for the selected central wavelength, that is, $\lambda_0 = 540$ nm. The obtained rainbow beam illuminates the phase SLM (*Holoeye* 1080P, 1,920 × 1,080 pixels, pixel pitch $\Delta p = 8$ μm), which is imaged by a magnifying 4F system comprising lenses L_1 ($F_1 = 100$ mm) and L_2 ($F_2 = 600$ mm). Additionally, at the focal plane of lens L_1, a vertical absorbing cut-off filter is placed and its position is adjusted to pass only first diffraction order of the SLM. The filter supports a complex coding scheme [24,25] implemented in hologram generation. In the conjugated SLM plane, there is a field lens L ($F = 600$ mm) that creates RVW at its focal plane.

Numerical processing is an integral part of the FRHD. The details of a rainbow hologram generation are explained in [17]. For the generation of the rainbow holographic content, the following four-step algorithm is implemented. First, the distribution of the complex object wave is calculated or captured at the VW plane of the display. For the generation of holograms of a 3D object, the 3D point-based CGH method is used [26,27], and for capturing of holograms of real object, the lensless Fourier hologram capture system is utilized [28]. Then, to reduce the spatial frequency content in vertical direction, the numerical slit is applied to the complex object wave field. The next step is the propagation from the VW plane to the SLM plane. Finally, the complex object wave is encoded into a phase-only hologram.

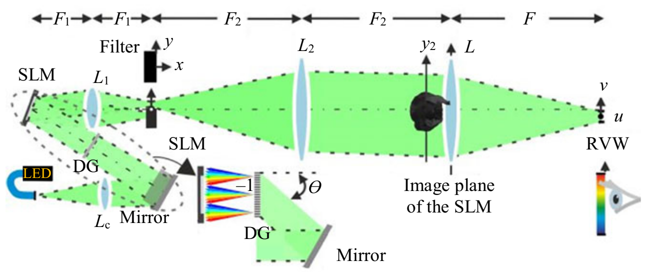

FIGURE 2 FRHD setup

3 | VISUAL PERCEPTION OF FOURIER RAINBOW HOLOGRAPHIC DISPLAY

In this section, we discuss the visual perception of the FRHD. Here, we focus on the viewing zone, FoV, and image blur of the FRHD. The first two concern visual comfort, while the last one is related to image resolution. For this purpose, in this section, we utilize WD [20] as an analysis tool for space-frequency representation.

3.1 | Viewing zone and multispectral FoV

For holographic displays, the size of the viewing zone for a large hologram is an important factor for the comfort of observation. Due to the small diffraction of the current SLM, the viewing zone of the holographic display is small and visual comfort is low. Especially, in a VW display, the viewing zone is very small and the image can be seen only from a limited position. The viewing zone is an area where the image generated by the entire SLM can be observed. Then, the viewing zone of the VW display is determined by two converging rays diffracted by the edge pixels of the SLM, as shown in Figure 3A.

In the FRHD, the multispectral reconstruction plane waves illuminate the SLM with different and specific incidence angles. Each reconstruction wave converges at the focal plane of the field lens at different transverse locations, and all reconstruction plane waves of the white-light source form an extended RVW in vertical direction. The SLM can diffract the light in the angular range, as illustrated in Figure 3 using dashed lines. Thus, the viewing zone of the FRHD is determined by two converging rays with different wavelengths diffracted from the edge pixels of the SLM, as shown in Figure 3B. The viewing zone of the FRHD is formed asymmetrically because the diffraction angle depends on the wavelength. Figure 3 compares the viewing zone of the VW display and FRHD. Note that the viewing zone of the FRHD is largely extended by rainbow illumination. The approximated size of the viewing zone is provided in [17].

Let us use a WD representation to analyze the extension of a viewing zone. According to the sampling theory, we assume that the holographic signal diffracted at the SLM is limited in frequency and spatial domains. Then, the signal boundary can be expressed as $B_x = N\Delta p$ and $B_f = 1/\Delta p$ [21]. In FRHD, B_f is smaller and is related to the size of the slit S applied within the hologram generation procedure, where $B_f = S/(F\lambda)$. As explained in Section 2, the FRHD is an extension of the VW display with rainbow illumination. Rainbow illumination is an angular multiplexing technique, which is an assembly of plane waves with different inclinations. For a specific wavelength λ, the illumination is a tilted plane wave. Its angle is determined by the period of diffraction grating and the angle θ from

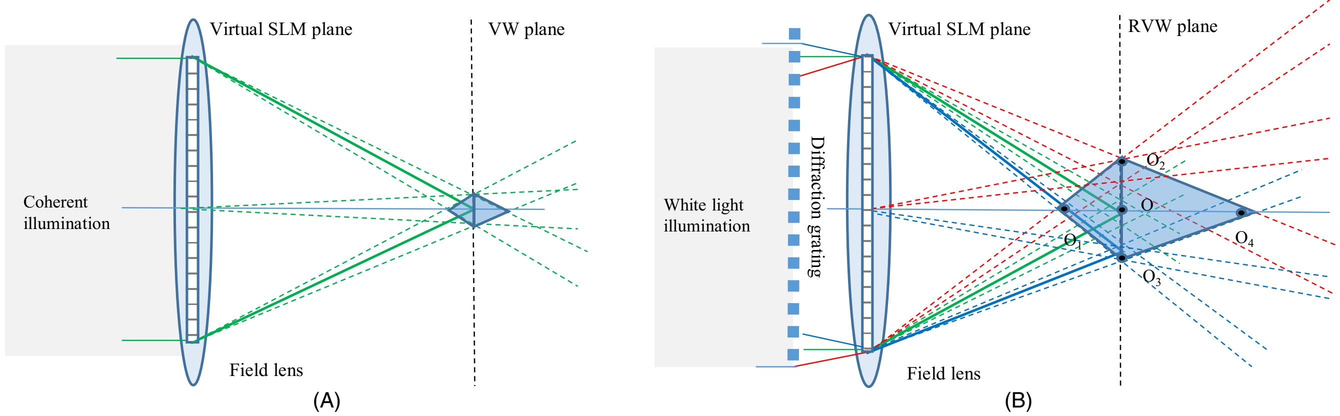

FIGURE 3 Viewing zone of (A) the VW display and (B) FRHD

Figure 2. The WD representation of the effect of inclined illumination for wavelength λ can be explained using a spectral frequency shift f_λ as:

$$W_\lambda(x,f) = W(x,f - f_\lambda). \tag{1}$$

The spectral shift f_λ is

$$f_\lambda = \left(\frac{1}{\lambda} - \frac{1}{\lambda_0}\right)\frac{\sin\theta}{M}, \tag{2}$$

where $M = F_2/F_1$ is the magnification ratio of the display system and λ_0 is the wavelength of the light incident to the SLM plane in normal direction. Figure 4 shows the effect of wavelength on the SLM bandwidth with dashed rectangles, which is expressed as a vertical shift on the frequency axis. The figure is drawn for a plane of the field lens.

According to the system shown in Figure 3B, the field lens is located at the image plane of the SLM. If the focal length of the field lens is F, the WD chart showing a change in the holographic signal due to the field lens can be expressed as:

$$W_{\text{lens}}(x,f) = W\left(x,\ f + \frac{x}{\lambda F}\right). \tag{3}$$

In Figure 4, WD shows the effect of the lens through transition from dashed to solid rectangles. The inclination angle of a sheared rectangle is determined by $1/(\lambda F)$. The color rectangle presented on the top corresponds to the boundary wavelength $\lambda_B = 460$ nm, while that on the bottom corresponds to the central wavelength $\lambda_0 = 540$ nm. In the analysis, we assume a chromatically corrected field lens.

When the eye is located at distance z_p from the SLM plane, the change in bandwidth of the signal diffracted on the SLM for wavelength λ can be represented as:

$$W_{z_p}(x,f) = W\left(x + \lambda z_p f, f\right). \tag{4}$$

At the observation plane, the eye pupil acts as an aperture, and thus, its WD can be represented by a rectangle, which is illustrated in Figure 5 by a dashed line. At the SLM plane, the effect of the eye can be explained by the backward Fresnel propagation of this eye pupil. When the distance between the SLM plane and the eye pupil plane is z_p, the WD chart for the eye pupil at the SLM plane can be expressed using (4) with $-z_p$. In Figure 5, the WD chart for the eye pupil at the observation plane is illustrated as sheared rectangles for selected wavelengths λ_B and λ_0. Here, the inclination angle of the corresponding rectangle is determined by $1/(\lambda z_p)$. The off-axis movement of the eye at the observation plane and SLM plane can be explained as a shift in x-direction. In Figure 5, each WD chart for EYE_{O3} can be simply expressed by shifting WD of EYE_O to the location of point O_3.

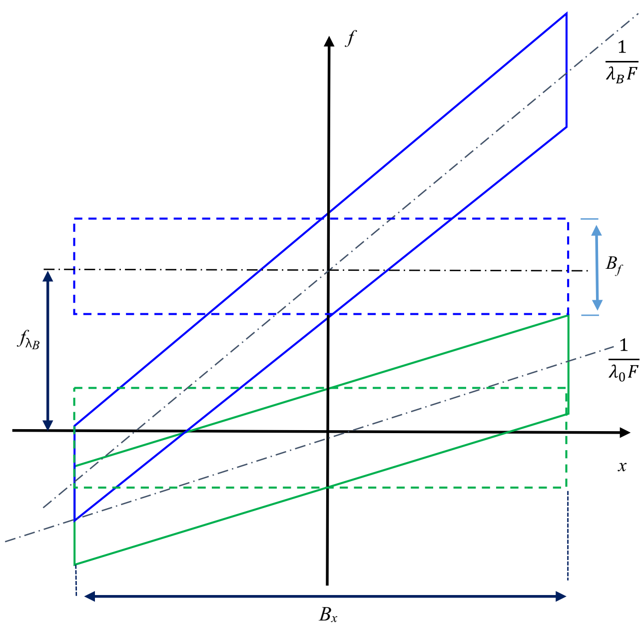

FIGURE 4 Illustration of the bandwidth evolution for the SLM plane as an effect of the field lens and rainbow illumination for two selected wavelengths

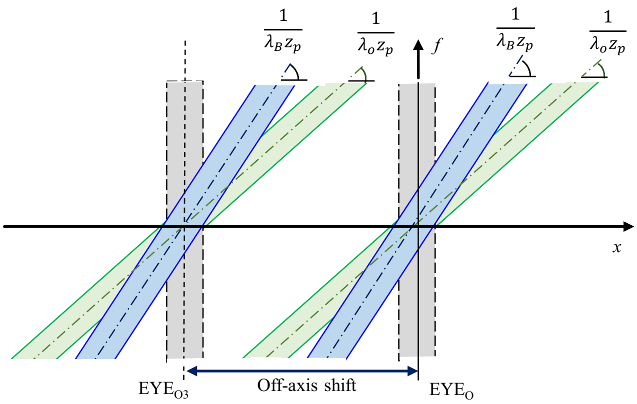

FIGURE 5 Illustration of the eye effect using WD at the SLM plane

The FRHD provides views of reconstruction with rainbow color within a large viewing zone. To understand multispectral properties of the FRHD, consider WD representations of the effect of the eye pupil and the signal reconstructed by the display. In Figures 6 and 7, the perceived image size and resolution for different wavelengths are analyzed using space-frequency WD. For this analysis, four observation points in the viewing zone, the center point O and three boundary points O_1, O_2, and O_3, are selected. In Figures 6 and 7, blue, green, and red solid rectangles represent WD charts for the display for three reconstruction plane waves with wavelengths $\lambda_B = 460$ nm, $\lambda_0 = 540$ nm, and $\lambda_R = 660$ nm, respectively. At the observer side, the eye pupil acts as the spatial filter. Figures 6 and 7 contain WDs of the eye pupil for different observation points calculated for the observation and SLM planes. The overlapping areas between WDs of the eye pupil and display are marked with corresponding colors and present the bandwidth captured by the eye.

Figure 6 illustrates WDs of the display and the eye pupil for the observation points O, O_2, and O_3 at the RVW plane ($z_p = F$). The distance between two boundary regions, EYE_{O2} and EYE_{O3}, is the size of the viewing zone in the vertical direction. For better illustration, Figure 6 is not drawn in scale. The plot in physical units gives the size of the viewing zone as 20.5 mm in the vertical direction.

The FoV of the display is the maximum size of the holographic view. The dimension of the perceived image is the size of the overlapping area of the WD charts of the eye pupil and the bandwidth of the display at the SLM plane. As shown in Figure 6B, when the eye is at the RVW plane, the WD diagram for the display and the eye pupil has the same inclination angle for each wavelength. As a result, a single-colored hologram can be perceived by the eye, and little information for different wavelengths is transmitted. According to the eye movement in vertical direction, a monochromic hologram with different color is provided with the same FoV. Figure 6 shows that the resolution of the single view is the highest for λ_B. At the same time, the spatial size of VW is the smallest for this wavelength.

Now, consider the case where the observer's eye is out of the RVW plane ($z_p \neq F$). For this observation condition, a view in rainbow colors is obtained. Figure 7A illustrates the WDs of the display and the eye pupil for the observation point O_1. At this position, the holographic signal with multiple colors is transmitted into the pupil. For the discussion, the same three wavelengths are considered. However, note that the spectrum is continuous. Figure 7B illustrates a change in the holographic signal of the FRHD from the RVW to the SLM plane and the multispectral property of the display for the observation point O_1. At the SLM plane, the tilt of the WD of the display is $1/(\lambda F)$, while that of the eye is $1/(\lambda z_p)$. Thus, the common area of both WDs, which is the size of view for this wavelength, is limited. The same happens for all wavelengths. The size of the view for wavelength λ can be expressed as:

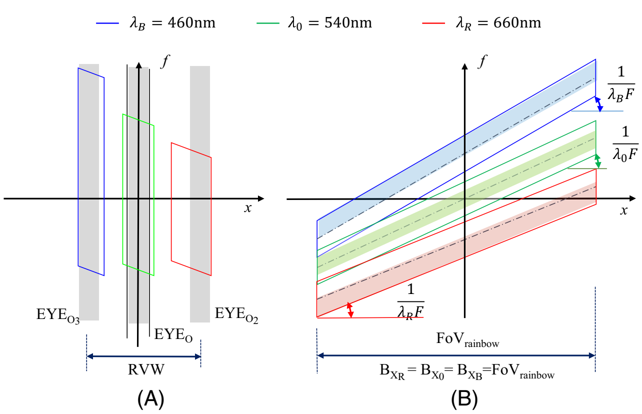

FIGURE 6 WD charts of the eye function and FRHD for observation points O, O_2, and O_3 (A) at the observation plane and (B) the SLM plane

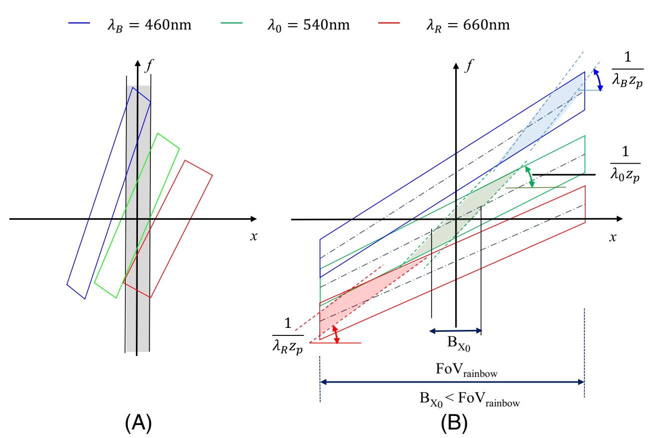

FIGURE 7 WD charts of the eye function and FRHD for the observation point O_1 (A) at the observation plane and (B) the SLM plane

$$\mathrm{B}_{x_\lambda} = \left| \min\left\{ \frac{Bx}{2}, \frac{\lambda z_\mathrm{p}}{1-\frac{z_\mathrm{p}}{F}}\left(f_\lambda + \frac{D}{2\lambda z_\mathrm{p}}\right) \right\} - \max\left\{ \frac{-Bx}{2}, \frac{\lambda z_\mathrm{p}}{1-\frac{z_\mathrm{p}}{F}}\left(f_\lambda - \frac{D}{2\lambda z_\mathrm{p}}\right) \right\} \right|, \tag{5}$$

where D is the size of the eye pupil. As shown in Figure 7, for point O_1, the position of the view is different for all wavelengths. For point O_1, all visible wavelengths generate the total FoV of the FRHD. For different points, the visible range is smaller. If we set the range of the visible wavelengths to $\{\lambda_-, \lambda_+\}$, the dimensions of the FRHD view can be expressed as:

$$\mathrm{FoV}_{\mathrm{Rainbow}} = \left| \min\left\{ \frac{B_\mathrm{x}}{2}, \frac{z_{\mathrm{p}\lambda_+}}{1-\frac{z_\mathrm{p}}{F}}\left(f_{\lambda_+} + \frac{D}{2z_{\mathrm{p}\lambda_+}}\right) \right\} - \max\left\{ \frac{-Bx}{2}, \frac{z_{\mathrm{p}\lambda_-}}{1-\frac{z_\mathrm{p}}{F}}\left(f_{\lambda_-} - \frac{D}{2z_{\mathrm{p}\lambda_-}}\right) \right\} \right|. \tag{6}$$

Figure 8 illustrates the extension of the FoV according to the spectral bandwidth of the analyzed light sources with central wavelength $\lambda_0 = 540$ nm and spectral bandwidths $\Delta\lambda = \lambda_+ - \lambda_-$. The selected sources consider a laser (0 nm), two LEDs (20 and 40 nm), and a white LED (200 nm). Each graph represents the size of FoV for different observation distances calculated with (6). The FoV of our display is presented using a blue solid line, where the marked points O_1 and O_4 indicate longitudinal size of the viewing zone of our system. Notably, the viewing zone analysis based on (6) is more accurate than that presented in our previous study [17], where paraxial approximation is applied for the angle of the white-light illumination beam.

3.2 | Image blur

Image blur, which is a measure of the resolution of rainbow hologram, is generated by geometrical displacements of the images reconstructed for different wavelengths.

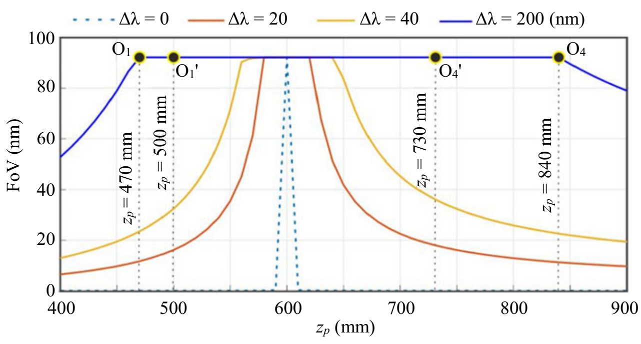

FIGURE 8 Illustration of the extension of FoV for the chosen spectral bandwidths of the light source

According to [19], image blur is a function of size of the slit and the eye pupil. The slit is a spatial frequency filter limiting frequency encoded in the hologram. In the rainbow display, the reconstructed waves for different wavelengths are transversally shifted at the observation planes, and thus, the pupil acts as a spectral filter.

Consider a simple observation case where an on-axis eye at the RVW plane views the reconstructed on-axis point located at distance z from the field lens. The WD of this point reconstructed with λ_0 is shown in Figure 9A with a red dotted line. The red solid line shows WD of the reconstructed point with wavelength λ_+. For this selected wavelength, the reconstructed wave is located outside of the eye pupil and focused at point P_+. Notably, using (2), this wave is reconstructed with the inclined plane wave of angle β:

$$\beta = \frac{D+S}{F} = \frac{(\lambda_0 - \lambda_+)\sin\theta}{M\lambda_0}. \tag{7}$$

Only object waves that are reconstructed with angles smaller than $|0.5\beta|$ are captured by an eye. The above equation immediately gives expressions for spectral content δ_λ and related image blur $\delta_{\delta\lambda}$ as:

$$\delta_\lambda = \frac{M\lambda_0}{\sin\theta}\left(\frac{D+S}{F}\right), \tag{8}$$

$$\delta_{\partial\lambda} \cong z\left(\frac{D+S}{F}\right). \tag{9}$$

Equations (8) and (9) were originally developed in [19] using ray analysis, where it is assumed that all reconstruction plane waves have the same wavelength. Here, the same approximation is used. The major strength of the rainbow display, as illustrated in Figure 3, is the large viewing zone. Therefore, in this section, formulas for the image blur and spectral content for the arbitrary location of the observer are found.

In this generalized geometry, the object point P is observed from the distance $z_\mathrm{p} \neq F$. In the Figure 9B, WD of the reconstructed object wave with wavelength λ_0 at z_p is shown using a red dotted line. The spatial extension of this wave is S' and its size is determined by the propagation from RVW to the observation plane. The red solid line shows WD of P_+' at z_p reconstructed with λ_+'. For this wavelength, the wave outside of the eye pupil is obtained. Similarly, as in the previous case, the angle of the reconstructing plane wave β' is related to the transverse and frequency shift as:

$$\beta' = \frac{D+S'}{z_\mathrm{p}} = \frac{D}{z_\mathrm{p}} + \frac{S(z+z_\mathrm{p})}{z_\mathrm{p}(z+F)} = \frac{(\lambda_0 - \lambda_+^{'})\sin\theta}{M\lambda_\mathrm{O}}. \tag{10}$$

Using this equation, the spectral content δ_λ and related image blur $\delta_{\delta\lambda}$ are

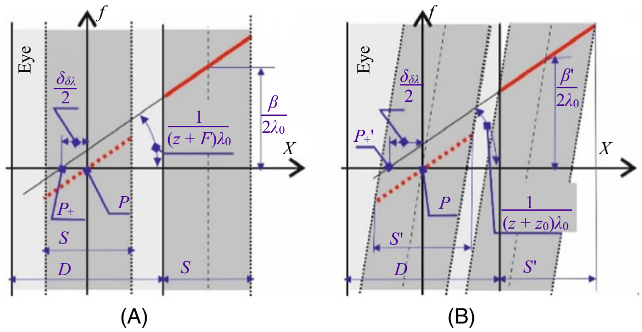

FIGURE 9 WD geometry for image blur analysis for (A) $z_p = F$ and (B) $z_p > F$

$$\delta_\lambda \cong \frac{M\lambda_0}{\sin\theta}\left(\frac{D}{z_p} + \frac{S(z+z_p)}{z_p(z+F)}\right), \tag{11}$$

$$\delta_{\partial\lambda} \cong z\left(\frac{D}{z_p} + \frac{S(z+z_p)}{z_p(z+F)}\right). \tag{12}$$

To provide quantitative assessment of the above results, the accuracy of (11) and (12) is numerically investigated. This observation of the reconstructed holograms generated for point objects of different axial locations and different slit sizes is numerically simulated. The observer's eye is simulated by 4 mm pupil at the observation plane. For each hologram, a set of intensity reconstructions for a range of wavelengths is calculated at the longitudinal location of the analyzed object point. The reconstructions are computed for white-light spectrum with 0.1 nm step and only for the light transmitted by the eye pupil.

The simulation results are presented in Figure 10. The left set of the figures presents image blur, while the right set shows the corresponding spectral contents. The rows are calculated for different widths of the slit and different locations of the point. The axial locations of the points are selected appropriately for the chosen widths of the slit. Each plot presents results calculated for three observation distances: 300 mm, 600 mm, and 900 mm. Notably, the selected distances are outside of the viewing zone. However, those on the axis points analyzed here are fully observable. Such large distances are selected to illustrate the accuracy of the formulas more precisely. The left plots, using solid lines, present the intensity distributions calculated with the simulation, while the dotted lines indicate values of image blur calculated with (12). The plots on the right present distributions of the spectra, which correspond to the reconstructions showed on the left. The dotted lines indicate the calculated values of δ_λ with (11). The simulation results presented in Figure 10 prove good accuracy of the developed measures given by (11) and (12).

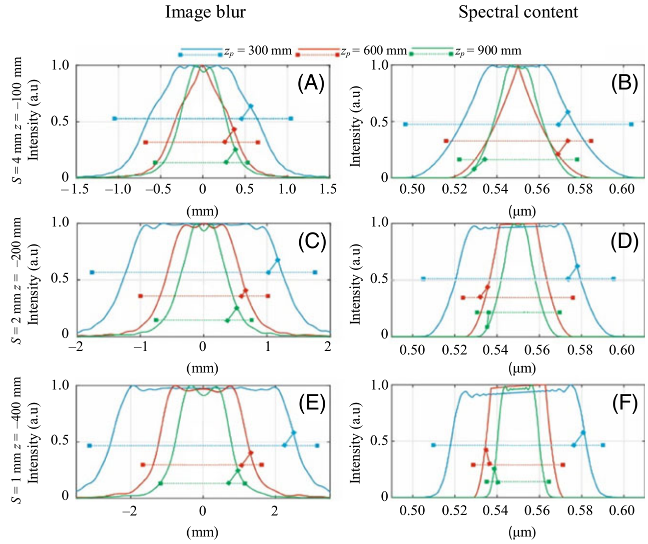

FIGURE 10 Illustration of accuracy of image blur (12) and spectral content (11); left column—image blur; right—spectral content; solid lines indicate simulation results; dotted lines present calculated measures δ_λ and $\delta_{\delta\lambda}$

4 | EXPERIMENTAL RESULTS

In this section, the visual properties of the FRHD are validated through two experiments. The first experiment focuses on visual comfort of the display and shows the FoV obtained for boundary positions of the viewing zone. The second illustrates the image blur of the display for different reconstruction distances and slit sizes. The images are directly taken by a *Cannon 5D* camera. The focal length and *f*-number, which defines the aperture size of the camera lens, are set to $F_{cam} = 43$ mm and *f*-number = 7.1. Using these values, the captured images are the most similar to the views seen by the observer [29]. However, for this setting, the camera is unable to capture images with the resolution perceived by the human eye.

The first experiment investigates the multispectral FoV of the display. For this purpose, the hologram of a 2D

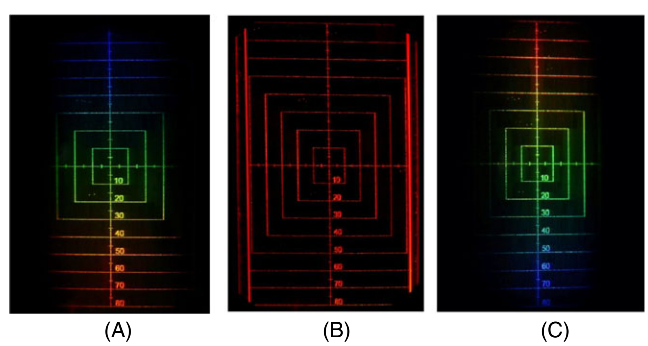

FIGURE 11 FoV at different observation positions: (A) O_1', (B) O_2', and (C) O_4'

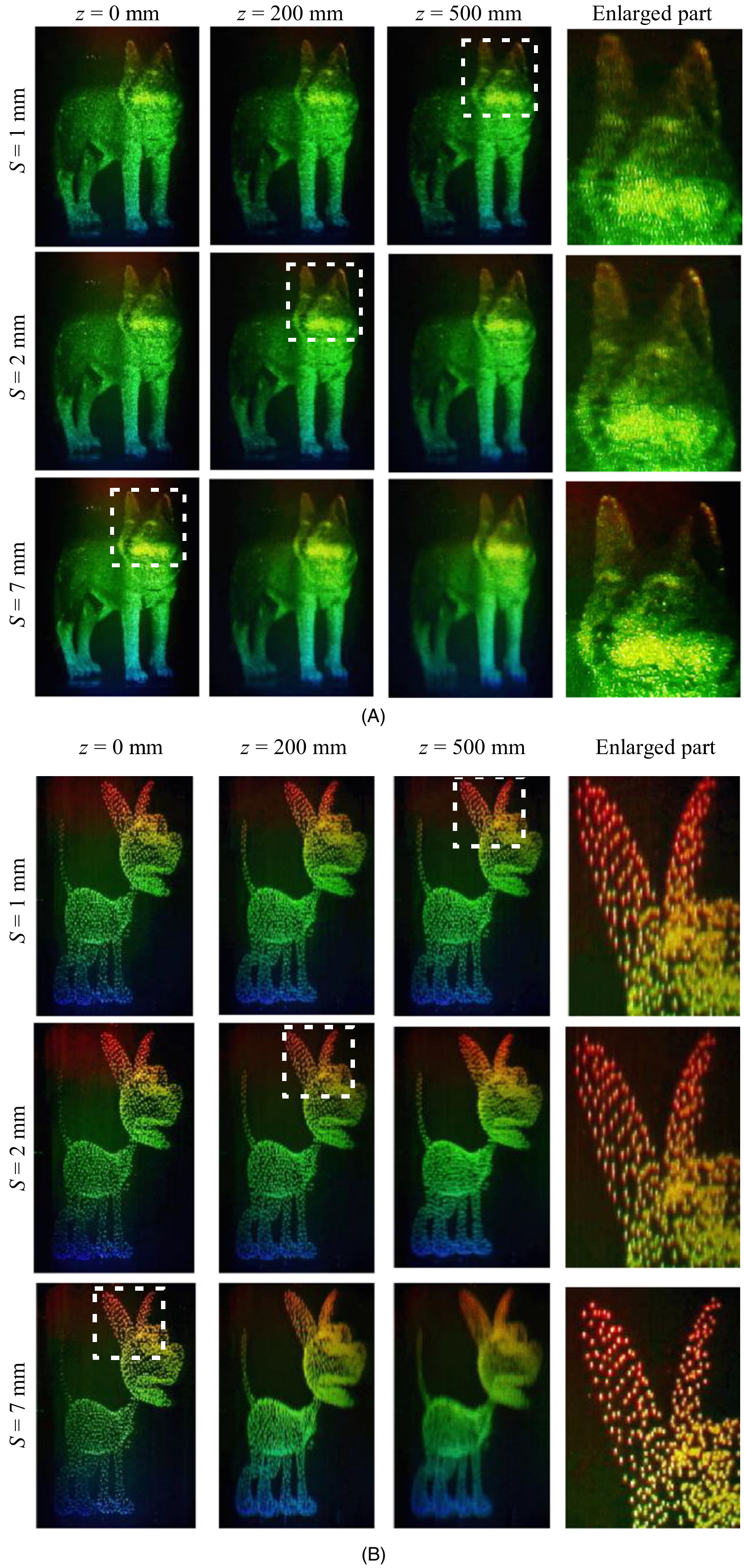

FIGURE 12 Illustration of effect of slit size and reconstruction distance on image blur of the FRHD for (A) DH of a real object and (B) CGH

chart is generated and optically reconstructed in the FRHD. The hologram is generated at the SLM plane for $\lambda_0 = 540$ nm. The reconstructed image is captured for boundary camera positions of the viewing zone. The 2D chart represents squares with different widths (see millimeter scale in the image). The maximum size of the square matches the SLM size. Figure 11 shows the views of optical reconstruction photographed from three boundary points O_1', O_2', and O_4' with coordinates (0, 0, 500), (0, 10, 0), and (0, 0, 730) (mm), respectively. These points, marked with prime symbol, are found experimentally and limit the size of the viewing zone of the display system. Their values are different from those obtained with the numerical analysis presented in Figure 8, which includes markings of points O_1' and O_4'. These discrepancies are the effect of insufficient numerical apertures of lenses L_1 and L_2. Thus, the boundary points of the view are reconstructed by a limited spectral range of the source.

The second experiment evaluates the effect of the slit size and reconstruction distance on the image blur in the FRHD. In this regard, the rainbow holograms of a real and a synthetic 3D object are generated and optically reconstructed for different slit sizes S (1 mm, 2 mm, and 7 mm) and reconstruction distances z (0 mm, 200 mm, and 500 mm). The parameters are chosen to demonstrate that the selection of the slit size allows to increase the imaging depth of the display at the expense of the resolution at the SLM plane. This experiment is not a quantitative measurement of the results obtained from (10) and (11). The camera used for capturing is unable to simulate the eye with sufficient accuracy. The captured image occupies a small area of the camera sensor. Thus, the resolution of the observed views with the eye pupil is always higher [17]. All holograms are generated for $\lambda_0 = 540$ nm. The first test object is “wolf” figurine with dimensions of 80 mm width, 60 mm height, and 30 mm depth, captured in the lensless Fourier capture system [28] with the following parameters: camera resolution 2,448 × 2,050; camera pixel pitch 3.45 μm; object distance from the camera 790 mm; registration wavelength 540 nm. The second object is a “dog” model represented by a cloud of points. It has dimensions of 50 mm width, 70 mm height, and 25 mm depth, and comprises 2,500 points. The obtained optical reconstructions are photographed by a camera placed at $z_p = 700$ mm, which is 100 mm out of RVW.

Figure 12 shows images captured for the chosen parameters. Additionally, in the last column, the enlarged parts of the most meaningful images are illustrated. The results show that a change in the slit size gives control over the resolution at the SLM plane. For large reconstruction distances, the selection of the correct slit size improves the quality of the observed reconstructions. For example, for a 7 mm slit size, the reconstruction depth is small. In contrast, for 1 mm slit size, the resolution is almost constant for all chosen reconstruction depths.

5 | CONCLUSIONS

The rainbow display allows for the reconstruction of large and real 3D orthoscopic objects [17]. Even though it does not reproduce real colors, the perceived views look interesting and impressive. The display provides views where color and resolution change with the movement of observer's eye. Therefore, in rainbow holography, visual perception plays a very important role.

In this study, visual perception of the rainbow holographic display is investigated using WD. The extension of the viewing zone of the display, including its multispectral FoV, is analyzed theoretically. For this purpose, a novel framework using WD analysis is proposed. The provided equation allows to calculate the size of FoV within and outside the viewing zone. Regarding the image quality, a quantitative assessment for image blur and spectral content are is introduced, which is another aspect of WD analysis. The accuracy of the developed measures is proved using numerical simulation. Optical reconstructions for the holograms of the computer model and the real object generated with different slit sizes, reconstruction distances, and observation conditions are shown to support the analysis experimentally.

ACKNOWLEDGMENTS

This study is extended from [18], which was presented in SPIE Photonics Europe 2018, Strasbourg, France.

ORCID

Hyon-Gon Choo https://orcid.org/0000-0002-0742-5429

REFERENCES

1. Y. Pan et al., *A review of dynamic holographic three-dimensional display: algorithms, devices, and systems*, IEEE Trans. Ind. Inform. **12** (2016), no. **4**, 1599–1610.
2. T. Kozacki et al., *Wide angle holographic display system with spatiotemporal multiplexing*, Opt. Express **20** (2012), 27473–27481.
3. J. Hahn et al., *Wide viewing angle dynamic holographic stereogram with a curved array of spatial light modulators*, Opt. Express **16** (2008), 2372–2386.
4. J. Son et al., *Holographic display based on a spatial DMD array*, Opt. Lett. **38** (2013), 3173–3176.
5. H. Sasaki et al., *Large size three-dimensional video by electronic holography using multiple spatial light modulators*, Sci. Rep. **4** (2014), 6177:1–6177:8.

6. Y. Lim et al., *360-degree tabletop electronic holographic display*, Opt. Express **24** (2016), 24999–25009.
7. J. Li, Q. Smithwick, and D. Chu, *Full bandwidth dynamic coarse integral holographic displays with large field of view using a large resonant scanner and a galvanometer scanner*, Opt. Express **26** (2018), 17459–17476.
8. Y. Takaki and K. Fujii, *Viewing-zone scanning holographic display using a MEMS spatial light modulator*, Opt. Express **22** (2014), 24713–24721.
9. S. Reichelt et al., Holographic 3-D displays electro-holography within the grasp of commercialization, in *Advances in Lasers and Electro Optics*, N. Costa and A. Cartaxo (eds), IntechOpen, London, UK, 2010.
10. T. Inoue and Y. Takaki, *Table screen 360-degree holographic display using circular viewing-zone scanning*, Opt. Express **23** (2015), 6533–6542.
11. Y. Sando, D. Barada, and T. Yatagai, *Holographic 3D display observable for multiple simultaneous viewers from all horizontal directions by using a time division method*, Opt. Lett. **39** (2014), 5555–5557.
12. Z. Zeng et al., *Full-color holographic display with increased-viewing-angle [Invited]*, Appl. Opt. **56** (2017), F112–F120.
13. A. Maimone, A. Georgiou, and J. S. Kollin, *Holographic near-eye displays for virtual and augmented reality*, ACM Trans. Graph. **36** (2017), no. 85, 1–16.
14. S. A. Benton and V. M. Bove, *Holographic Imaging*, John Wiley & Sons, Hoboken, NJ, USA, 2008, 145–172.
15. H. Yoshikawa and H. Taniguchi, *Computer generated rainbow hologram*, Opt. Rev. **6** (1999), 118–123.
16. H. Yoshikawa and T. Yamaguchi, *Computer-generated holograms for 3D display*, Chin. Opt. Lett. **7** (2009), 1079–1082.
17. T. Kozacki, M. Chlipala, and H. Choo, *Fourier rainbow holographic display*, Opt. Express **26** (2018), 25086–25097.
18. H. Choo, M. Chlipala, and T. Kozacki, *Image blur and visual perception for rainbow holographic display*, Proc. SPIE **10679** (2018), 106790S:1–106790S:7.
19. J. C. Wyant, *Image blur for rainbow holograms*, Opt. Lett. **1** (1977), 130–132.
20. M. J. Bastiaans, *Wigner distribution function and its application to first-order optics*, J. Opt. Soc. Am. **69** (1980), 1710–1716.
21. T. Kozacki, *On resolution and viewing of holographic image generated by 3D holographic display*, Opt. Express **18** (2010), 27118–27129.
22. L. Shi et al., *Near-eye light field holographic rendering with spherical waves for wide field of view interactive 3D computer graphics*, ACM Trans. Graph **36** (2017), no. 6, 236:1–236:17.
23. G. Finke, M. Kujawińska, and T. Kozacki, *Visual perception in multi SLM holographic displays*, Appl. Opt. **54** (2015), 3560–3568.
24. X. Li et al., *3D dynamic holographic display by modulating complex amplitude experimentally*, Opt. Express **21** (2013), 20577–20587.
25. T. Kozacki and M. Chlipala, *Color holographic display with white light LED source and single phase only SLM*, Opt. Express **24** (2016), 2189–2199.
26. J.-H. Park, *Recent progress in computer-generated holography for three-dimensional scenes*, J. Inform. Displ. **18** (2017), 1–12.
27. A. Symeonidou, D. Blinder, and P. Schelkens, *Color computer-generated holography for point clouds utilizing the Phong illumination model*, Opt. Express **26** (2018), 10282–10298.
28. T. Kozacki, M. Chlipala, and P. L. Makowski, *Color Fourier orthoscopic holography with laser capture and an LED display*, Opt. Express **26** (2018), 12144–12158.
29. R. Cicala, *The Camera Versus the Human Eye*, PetaPixel, Nov. 17, 2012. https://petapixel.com/2012/11/17/the-camera-versus-the-human-eye

AUTHOR BIOGRAPHIES

Hyon-Gon Choo received his BS and MS degrees in electronic engineering in 1998 and 2000, respectively, and his PhD in electronic communication engineering in 2005 from Hanyang University, Seoul Korea. He is currently working as a Principal Researcher in Electronics and Telecommunications Research Institute, Daejeon, Korea. His research interests include digital holography, holographic display, computer vision, and 3D broadcasting technologies.

Maksymilian Chlipala received his MS degree in photonics engineering from the Faculty of Mechatronics, Warsaw University of Technology, Warsaw, Poland, in 2013. In 2013, he began PhD studies at Faculty of Mechatronics, Warsaw University of Technology, in the area of construction and exploitation of machines. His main research interests are digital holography, holographic displays, spatial light modulators, and speckle reduction with LED sources.

Tomasz Kozacki received the PhD (2005) and DHs (2013) in photonics from the Warsaw University of Technology, Poland. Since 2003, he has been with the Department of Mechatronics, Photonics Engineering Division, where he is now a professor. His scientific research is related to digital holography, holographic displays, holographic microscopy, computational diffraction, and holographic tomography. He has authored and co-authored more than 50 scientific journal publications and more than 90 papers in conference proceedings.